Accepted Manuscript

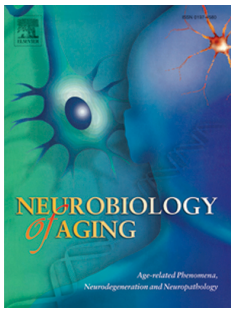

Amyloid load and TSPO in APPswePS1-dE9 mice: a longitudinal study

Sophie Sérrière, Clovis Tauber, Johnny Vercouillie, Céline Mothes, Christelle Pruckner, Denis Guilloteau, Michael Kassiou, Aurélie Doméné, Lucette Garreau, Guylène Page, Sylvie Chalon

PII: S0197-4580(15)00041-X

DOI: 10.1016/j.neurobiolaging.2014.11.023

Reference: NBA 9188

To appear in: *Neurobiology of Aging*

Received Date: 15 July 2014

Revised Date: 3 November 2014

Accepted Date: 25 November 2014

Please cite this article as: Sérrière, S., Tauber, C., Vercouillie, J., Mothes, C., Pruckner, C., Guilloteau, D., Kassiou, M., Doméné, A., Garreau, L., Page, G., Chalon, S., Amyloid load and TSPO in APPswePS1-dE9 mice: a longitudinal study, *Neurobiology of Aging* (2015), doi: 10.1016/j.neurobiolaging.2014.11.023.

Amyloid load and TSPO in APPswePS1-dE9 mice: a longitudinal study

Sophie Sérrière[a], Clovis Tauber[a], Johnny Vercouillie[a], Céline Mothes[b], Christelle Pruckner[a], Denis Guilloteau[a,c] Michael Kassiou[d], Aurélie Doméné[a], Lucette Garreau[a], Guylène Page[e*], Sylvie Chalon[a*§]

[a]UMR Inserm U930, Université François-Rabelais de Tours, 37000 Tours, France

[b]Laboratoires Cyclopharma, 37000 Tours, France

[c]CHRU de Tours, 37000 Tours, France

[d]School of Chemistry and Faculty of Health Sciences, University of Sydney, Sydney, Australia

[e]EA 3808 CiMoTheMA, Université de Poitiers, TSA5115, 86073 Poitiers, France

*Both authors contributed equally to this work

[§]Corresponding author: Sylvie Chalon, UMR Inserm U930, UFR de Médecine, 10 boulevard Tonnellé, 37032 Tours Cedex 01, France

Tel 33(0) 2 47 36 72 43

Fax 33(0)2 47 36 72 24

e-mail: sylvie.chalon@univ-tours.fr

Abstract

We studied concomitantly the level of neuroinflammation and Aβ load in the APPswePS1dE9 transgenic mouse model of Alzheimer's disease using PET imaging. The TSPO tracer [^{18}F]DPA-714 was used to measure neuroinflammation and [^{18}F]AV-45 for Aβ load in mice at 6, 9, 12, 15 and 19 months of age. At 19 months, we also analysed the neuroinflammatory and neuroanatomical status of mice brains. Imaging experiments showed that the main affected brain areas were the cortex and to a lesser extend the hippocampus, with a concomitant progression of neuroinflammation with increased amyloid burden. At 19 months, it was interesting to note that no increase in TSPO binding was observed in the cerebellum while immunostaining revealed W0-2-positive plaques. This indicated that in this region the amyloid deposits seemed not be a stimulator of inflammation. This was in agreement with the level of microglia and astrocytes staining that were observed. Our findings provide a better understanding of the relationships between neuroinflammation and plaque accumulation in the course of the disease in this mouse model. The monitoring of both processes should be of value to validate potential therapeutic approaches.

Key-words: Alzheimer's disease; Amyloid load; Neuroinflammation; PET

1. Introduction

The impact of Alzheimer's disease (AD) in terms of number of affected people and lack of efficient treatment makes it one of the most challenging diseases. AD is characterized by several neuropathological hallmarks such as accumulation of extracellular β-amyloid (Aβ) plaques, intracellular neurofibrillary tangles of hyperphosphorylated tau protein, and loss of neurons (Braak and Braak 1991).

An involvement of neuroinflammation in AD is well accepted (Akiyama et al. 2000; Heneka et al. 2010) and several mechanisms are proposed to explain interactions between the neurodegeneration and neuroinflammatory processes. The concept that glia-induced inflammation is an amplifier of pathology suggests that inhibition or modulation of neuroinflammation could result in reduction of neurodegeneration (Glass et al. 2010). In AD research, the concomitant study of these processes could provide broader insights into disease pathogenesis. Molecular imaging methods such as positron emission tomography (PET) provide the opportunity to perform this type of investigation, through in vivo exploration of specific molecular targets with the use of radioactive tracers. The development of PET systems adapted to small animals has substantially increased during the last decade, thus expanding the use of this methodology in animal models of brain disorders.

The inflammatory reaction in the brain involves the activation of microglia (Kreutzberg 1996) leading to a dramatic increase in the expression of the translocator protein 18 kDa (TSPO) which can be considered as a sensitive biomarker of microglial activation (Chen and Guilarte 2008). The most widely PET tracer for TSPO exploration is [^{11}C]PK-11195, both in preclinical and clinical studies (Venneti et al. 2006), but a number of compounds labelled with [^{18}F], which have the advantage of a longer half-life than [^{11}C], are now available. Among these tracers, [^{18}F]DPA-714 has demonstrated its utility in several animal models

(James et al. 2008; Chauveau et al. 2009; Boutin et al. 2013) and human brain disorders (Corcia et al. 2012).

Several PET tracers for Aβ plaques are also available such as the prototype, [^{11}C]PIB (Klunk et al. 2004), and several more recent [^{18}F]-labelled tracers including [^{18}F]AV-45 or florbetapir (Choi et al. 2009) which is now used in clinical studies (Wong et al. 2010 ; Clark et al. 2011 ; Fleisher et al. 2011 ; Camus et al. 2012 ; Joshi et al. 2012 ; Rosenberg et al. 2013).

The co-existence of reliable PET imaging methods with dedicated tracers in small animals and relevant animal models of AD is an opportunity to better understand the pathophysiological mechanisms of the disease and to monitor potential therapeutic approaches. In this study, we assessed concomitantly the neuroinflammation and development of Aβ accumulation as disease markers, in a longitudinal study, using a mouse model of AD. We utilized the APPswePS1dE9 transgenic (Tg) mouse model of amyloidosis (Jankowski et al. 2004), which is also characterized by a progressive inflammatory response and a degeneration of monoaminergic afferents and cognitive disorders (Liu et al. 2008; Ruan et al. 2009; Couturier et al. 2012; Zhang et al. 2012; O'Leary et al. 2009; Savonenko et al. 2005).

We explored longitudinally in each Tg and WT mouse the density of TSPO and Aβ load using PET imaging with [^{18}F]DPA-714 and [^{18}F]AV-45, respectively, at 6, 9, 12, 15 and 19 months of age. At 19 months, we also analysed the neuroinflammatory and neuroanatomical status of mice brains.

2. Materials and methods

2.1. Chemical products

Sodium fluoride (NaF), phenylmethylsulfonyl fluoride (PMSF), protease and phosphatase inhibitor cocktails, dithiothreitol (DTT), Paraformaldehyde (PFA), 4',6-diamidino-2-phenylindole (DAPI) and all reagent-grade chemicals for buffers were purchased from Sigma

(St Quentin Fallavier, France); NuPAGE® LDS 4X LDS Sample Buffer, NuPAGE® Sample Reducing Agent (10X), Novex® 4-20% Tris-glycine Mini gels, Novex® Tris-Glycine SDS Running buffer, Seeblue® Plus2 pre-stained standard, iBlot® Gel Transfer Device (EU), and Quant-it® protein assay from Gibco-Invitrogen (Fisher Bioblock Scientific distributor, Illkirch, France). For western blot, primary antibodies and secondary anti-rabbit IgG antibody conjugated with Horseradish Peroxydase (HRP) were purchased from Cell Signalling (Ozyme, St Quentin Yvelines, France) except antibody against Peripheral benzodiazepine receptor (PBR) or translocator protein of 18kDa (TSPO) purchased from Novus Biologicals® (Interchim distributor, Montluçon, France), anti-β actin from Sigma (St Quentin Fallavier, France), HRP-conjugated anti-mouse IgG from Amersham Biosciences (Orsay, France). For immunofluorescence, anti-glial fibrillary acidic protein (GFAP) antibodies were purchased from Cell Signalling (Ozyme, St Quentin Yvelines, France), macrosialin or murine homologue of the human CD68 from AbD Serotec (Düsseldorf, Germany), anti-amyloid peptide (clone W0-2, recognizes amino acids residues 4-10 of Aβ) from Millipore (St Quentin-Yvelines, France); fluorescent mounting medium and pencil Dakopen® from DakoCytomation, (Trappes, France). IgG- and protease-Free Bovine Serum Albumin (BSA) and secondary antibodies from Jackson ImmunoResearch Europe Ltd (Interchim, Montluçon, France).

2.2. Animals

Animals were treated in accordance with the European Community Council Directive 2010/63/EU for laboratory animal care and the experimental protocol was validated by the Regional Ethical Committee (Authorization n°2013-01-23).

Male hemizygote B6C3-Tg(APPswe, PS1dE9)85Dbo (Stock # 004462) and female wild-type mice (B6C3F1, Stock # 10010) were obtained from Jackson Laboratories (Bar Harbor, Maine

USA) and bred to create colonies of APPswePS1dE9 (Tg) and wild-type (WT) mice. As described in the web site of Jackson laboratory, two expression plasmids (Mo/HuAPP695swe and PS1dE9) were designed to each be controlled by independent mouse prion protein (PrP) promoter elements, directing transgene expression predominantly to central nervous system (CNS) neurons. The Mo/HuAPP695swe transgene expresses a "humanized" mouse amyloid beta (A4) precursor protein gene modified at three amino acids to reflect the human residues and further modified to contain the K595N/M596L mutations linked to familial Alzheimer's disease (FAD). The PS1dE9 transgene expresses a mutant human presenilin 1 carrying the exon-9-deleted variant (PSEN1dE9) associated with FAD. It is known that female displayed a more extensive phenotype than male and experience for over 6 years we have seen an untimely death in females with more frequent epileptic behavior compared to males. Thus, only male were included in this longitudinal study until 19-months of age.

A total of 10 male mice were included (5 Tg, 5 WT). They were individually housed under standard enriched environment in a room with a 12h/12h light/dark cycle (lights on from 7:00 to 19:00) under steady temperature (21 ± 1°C) and humidity (55 ± 5%) with access to food and water ad libitum.

2.3. Preparation of tracers

[^{18}F]AV-45 (Florbetapir) was prepared by the nucleophilic substitution of a tosylate precursor (E)-2-(2-(2-(5-(4-(tert-butoxycarbonyl(methyl)amino)styryl)pyridin-2yloxy)ethoxy)ethoxy) ethyl-4-methylbenzenesulphonate (AV-105) provided by Avid Radiopharmaceuticals (Philadelphia, PA) with a GMP certificate, on an automatic synthesizer according to previously described methods (Liu et al. 2010). Nucleophilic substitution was followed by hydrolysis of the BOC group, HPLC purification and formulation to afford [^{18}F]AV-45 with

40-55% yields decay corrected. The radiochemical purity and specific activity were 98% and 35 ± 5 GBq/μmol, respectively.

[^{18}F]DPA-714 N,N-diethyl-2-(2-(4-(2-fluoroethoxy)phenyl)-5,7-dimethyl-pyrazolo[1,5-α]pyrimidin-3-yl)acetamide (DPA-714) was labelled with fluorine-18 at its 2-fluoroethyl moiety, following nucleophilic substitution of the corresponding tosylate analogue, according to slight modifications of previously reported procedures (James et al. 2008). After purification, [^{18}F]DPA-714 was eluted by injectable ethanol, and saline was added to obtain an intravenously injectable solution (10% maximum in volume for ethanol). The radiochemical yields were 50-65% decay corrected. The radiochemical purity and specific activity were 98% and 68 ± 12 GBq/μmol, respectively.

2.4. PET imaging and data analyses

PET acquisitions were performed on a microPET eXplore VISTA-CT system (GE Healthcare, France) which has an effective axial/transaxial FOV of 4.8/6.7 cm, a spatial resolution less than 2 mm and a sensitivity above 2.5% in the whole FOV. Animals were anesthetized using isoflurane (Baxter, France), at 4-5% in O_2 for induction and then 1.5-2% during scan. Each mouse was scanned with [^{18}F]AV-45 and [^{18}F]DPA-714 with a maximal delay of 1 week between both, at the age of 6, 9, 12, 15 and 19 months. They were placed on a thermo-regulated bed (Minerve, France) in prone position with a nose cone. The brain was positioned on the center of the FOV. Before PET acquisition, a 5 min CT-scan was acquired for attenuation correction. Animals received into the tail vein a bolus injection of 20 MBq of [^{18}F]AV-45 or [^{18}F]DPA-714 in saline. During PET acquisition, the respiratory rate and body temperature were monitored and kept as constant as possible.

Each acquisition lasted 50 min and PET list-mode scans were rebinned into 27 frames: 4 frames of 10-seconds followed by 4 of 20-seconds, 4 of 60-seconds, 14 of 180-seconds, and 1

of 120-seconds. Each scan was corrected for randoms, scatter and attenuation, and the images were reconstructed using a 2D OSEM algorithm (GE Healthcare, France) into voxels of 0.3875 × 0.3875 × 0.775 mm^3. All images were analyzed using PMOD (3.403, PMOD Technologies, Zurich, Switzerland, www.pmod.com).

We applied partial volume correction on all PET images. We used a Reblurred Van Cittert (RVC) approach (Carasso 1999). The images were corrected with an in-house matlab implementation of the method, using the following algorithm (Tohka and Reilhac 2008):

$$t^{(k+1)} = t^{(k)} + \alpha\left(h * \left(i - h * t^{(k)}\right)\right)$$

$$t^{(0)} = i$$

Where the image $t^{(k)}$ is the estimation of the solution at iteration k , h is the point spread function (PSF) kernel, i the initial image, * denotes the convolution operator and $\alpha \in (0,2)$ is the step length.

Requirements of this method thus consist of a parameter α and of an invariant PSF within the system. In this study we set α=1, and used an estimation of the system PSF using point sources of radioactivity. The system PSF was slightly narrowed to avoid Gibbs ringing artifacts. For each PET image, 10 iterations of RVC algorithm were used. The PVE corrected images were used for standard uptake value (SUV) calculations. In this study, the standard uptake value ratio (SUVr) was used as semi-quantitative criterion. All SUVrs were calculated using the cerebellum as reference region.

For each PET scan, the data were summed over the first 5 minutes after radiotracer injection to create a pseudo perfusion image. This image reflects the initial flow-dependent activity and was registered with the CT image through a hardware registration known (PET to CT transformation). CT scans were also registered with a mouse brain MRI-Template (Mirrione, PMOD) and a mouse brain MRI-Template to CT transformation was saved. All PET images, after checking for potential head movements, were co-registered in a single interpolation to

the Mirrione mouse brain MRI Template by a combination of these two transformations (MRI Template to CT and PET to CT transformations). The inverse combined transformation was calculated. The Mirrione MRI template was processed in the PET space images using the inverse transformation applied on the originals dynamic PET data and the regions of interest (ROIs) statistics were extracted. PET images were analyzed with the ROIs for cortex, hippocampus, striatum and cerebellum.

2.5. Post-mortem experiments

After the last imaging studies at 19 months of age, mice were sacrificed by decapitation under light isoflurane anesthesia, and their brains carefully removed on ice. One half hemisphere was immediately frozen in isopentane cooled at -35°C. Sagittal sections (8 µm thickness for immunofluorescence and 16 µm thickness for autoradiography) were then cut in a cryostat microtome (Jung CM 3000, Leica) and thaw-mounted on Super-Frost Plus1 slides (CML, Nemours, France). Sections were kept at -80°C until use, and immunohistochemical and autoradiographic experiments were performed on consecutive sections from each brain.

The other hemisphere was dissected on ice in different brain regions, i.e. the temporal cortex, hippocampus, striatum and cerebellum which were immediately frozen in liquid nitrogen and kept at -80°C until use. Tissue of each area was thawed in 10 volumes of lysis buffer (25 mM Tris–HCl, 150 mM NaCl, 1 mM EDTA, pH 7.4) and supplemented with 50 mM NaF, 1 mM PMSF, protease and phosphatase inhibitor cocktails (50 µL/g of tissue and 10 µL/mL of lysis buffer, respectively) homogenized with a rod for Thomas's Potter (800 rpm) as previously described (Couturier et al. 2012). Lysates were sonicated and centrifuged at 15,000*g* for 15 min at 4°C. The resulting supernatants (dilution 1/200) were collected to measure the quantity of total protein with the Qubit® fluorescence detector (Life Technologies, Saint Aubin,

France). Samples were stored at -80°C until Western blot (WB) analysis and ELISA assay as described below.

2.5.1. Autoradiographic studies

The density of TSPO binding sites was measured by in vitro autoradiographic experiments using [^{3}H]PK-11195 (Specific Activity 3.06 GBq/µmol, Perkin Elmer) at 1 nM in 50 mM Tris HCL buffer pH 7.4. Brain sections were allowed to equilibrate at room temperature for 3h, then incubated with 1 nM [^{3}H]PK-11195 in 50 mM Tris-HCl buffer pH 7.4 at room temperature for 60 min. Nonspecific binding was assessed in the presence of 1 µM PK-11195 (Sigma Aldrich, France).

Slides were rinsed twice in ice cold buffer (4°C) for 4 min, then briefly in distilled water at 4°C and dried at room temperature. Dry slides were made conductive by an application of metal electric tape (3 M, Euromedex) on the free side and then placed in the gas chamber of the β-imager^{TM} 2000 (Biospace Lab, Paris, France). Data from brain sections were collected during 2 h. Four anatomical regions of interest, i.e. the cortex, hippocampus striatum and cerebellum were selected manually and identified in the Franklin and Paxinos atlas (2008). Using the β-vision software (Biospace Lab, Paris, France), the level of bound radioactivity was directly determined by counting the number of β-particles emitted from the delineated area. The radioligand signal in the ROIs was measured on at least eight sections for each mouse and expressed as counts per minute per square millimeter (cpm/mm^2). Specific binding was determined by subtracting nonspecific binding from total binding.

2.5.2. Immunofluorescent studies

Sagittal sections (8 µm thickness) were thawed in a solution of 4% PFA at 4°C for 30 min. Then the sections were washed three times in PBS for 5 min at room temperature (RT) and

delineated using the pencil Dakopen on the glass slide. Tissue sections were incubated for 1 h at RT in a buffer to enhance cell permeability and to block nonspecific sites (PBS/0.3% Triton X-100/5% BSA) before incubation overnight at 4°C either with monoclonal mouse W02 clone (1:100) or rabbit anti-GFAP (1:100) or rat anti-CD68 (1:50) or monoclonal rabbit-TSPO (1:100). Antibodies were diluted in PBS/0.3% triton X-100/1% BSA. After two washes with PBS at RT for 5 min, sagittal sections were incubated 1h at RT with secondary antibodies each at a 1:50 dilution in PBS/0.3% triton X-100/1% BSA: either donkey anti-mouse-Alexa 488 or donkey anti-rabbit-RRX or goat anti-rat RPE (STAR73 Serotec). The slices were washed twice for 5 min in PBS and twice for 5 min in distilled water and incubated with DAPI (1 µg/mL) for 15 min. After 3 washings in distilled water, the slices were mounted with fluorescent mounting medium and stored in a dark box at 4°C until observations and analysis.

Multiple labelled samples were examined with a spectral confocal FV-1000 station installed on an inverted microscope IX-81 (Olympus, Tokyo, Japan) with Olympus x40 oil, 1.2 NA, objective lens with optical section separation (z-interval) of 0.6 µm. Fluorescence signal collection, image construction, and scaling were performed using the control software (Fluoview FV-AS10, Olympus). Multiple fluorescence signals were acquired sequentially to avoid cross-talk between image channels. Fluorophores were excited with 405 nm line of a diode (for DAPI), 488 nm line of an argon laser (for Alexa 488), 543 nm line of a HeNe laser (for RPE or RRX). Emitted fluorescence was detected through spectral detection channels between 425-475 nm and 500-530 nm, for blue and green fluorescence, respectively and through a 560 nm long pass filter for red fluorescence. The images then were merged as an RGB image. Signals were analyzed by using Image J software (v 1.47). As for autoradiographic studies, four anatomical ROIs (temporal cortex, hippocampus, striatum and cerebellum) were selected manually and identified in the Franklin and Paxinos atlas (2008).

Measurements are performed on threshold images and corresponding raw integrated densities (sum of pixel values) were recorded.

2.5.3. Western blot studies

Samples (40 µg proteins) were prepared for electrophoresis by adding NuPAGE® 4X LDS sample buffer and NuPAGE® Sample Reducing Agent (10X). Samples were then heated up 100°C for 5 min, loaded into Novex® 4-20% Tris-Glycine mini Gels, run at 150 V for 60 min in Novex® Tris-Glycine SDS Running Buffer. Gels were transferred to nitrocellulose membranes using the iBlot® Dry blotting system set to program 20V for 7 min. Membranes were washed for 10 min in Tris-buffered saline/Tween (TBST: 20 mM Tris-HCl, 150 mM NaCl, pH 7.5, 0.05% Tween 20) and aspecific antigenic sites were blocked 2h in TBST containing 5% BSA.

Blots were incubated with primary antibody in blocking buffer overnight at 4°C. Antibodies used were monoclonal mouse anti-Aβ (clone W0-2), monoclonal rabbit anti-TSPO, mouse anti-GFAP at a dilution 1:1000. Membranes were washed twice with TBST and then incubated with the HRP-conjugated secondary antibody anti-rabbit IgG or anti-mouse IgG (1:1000), during 1 hour at RT. Membranes were washed again and exposed to the chemiluminescence Luminata Forte Western HRP Substrate (Millipore, Saint-Quentin-en-Yvelines, France) followed by signal's capture with the Gbox system (GeneSnap software, Syngene, Ozyme distributor). After 2 washes in TBST, membranes were probed with mouse antibody against β-actin (1:100000) overnight at 4°C. They were then washed with TBST, incubated with HRP-conjugated secondary antibody anti-mouse (1:1000) for 1h, exposed to the chemiluminescence Luminata classico substrate (Millipore, Saint-Quentin-en-Yvelines, France) and signals were captured. Automatic image analysis software is supplied with Gene

Tools (Syngene, Ozyme distributor). Ratios protein/β-actin were calculated and showed in the corresponding figures.

2.5.4. Pro-inflammatory cytokine ELISA

Commercially available ELISA kits were used for assessing IL-1β (sensitivity: 16 pg/mL) TNF-α (sensitivity: 4 pg/mL) and IL-6 (sensitivity: 2 pg/mL) according to the manufacturers' instructions (BioLegend, Ozyme, St Quentin Yvelines, France). The range of analysis was between 31.3-2,000 pg/mL for IL-1β and 7.8-500 pg/mL for TNF-α and IL-6. Homogenates from brain tissue (100 mg of tissue/mL) were added in each well of pre-coated plates and all steps were performed at room temperature (RT). The enzymatic reaction was stopped after 15 min incubation with tetramethylbenzidine (TMB) substrate by adding 2N H_2SO_4 and the optical density (OD) was read at 450 nm within 30 min, using the Multiskan® spectrum spectrophotometer. The cytokine levels were then calculated by plotting the OD of each sample against the standard curve. The intra- and inter-assay reproducibility was > 90%. OD values obtained for duplicates that differed from the mean by greater than 10% were not considered for further analysis. For convenience, all results are expressed in pg/mg protein.

2.5.5. Aβ-42 ELISA

Levels of Aβ42 were quantified using commercial ELISA kit (Invitrogen, Illkirch, France). Freshly frozen brain tissues were homogenized in 8 volumes of guanidine–Tris buffer (5 M guanidine HCl/50 mM Tris–HCl, pH 8.0). Then, homogenates were stirred for 4h on a vortex to maximum speed before they were assayed. Samples were diluted in cold BSAT-DPBS reaction buffer (0.2 g/L KCl, 0.2 g/L KH_2PO_4, 8.0 g/L NaCl, 1.15 g/L Na_2HPO_4, 5% BSA, 0.03% Tween-20, pH 7.4) supplemented with Protease Inhibitor Cocktail. Samples were centrifuged at 16,000*g* for 20 min at 4°C. The supernatant was diluted in standard diluents

buffer available in the kit. The final concentration of AEBSF (protease inhibitor in cocktail of proteases) was 1 mM in order to prevent proteolysis of Aβ peptides. The human Aβ42 standard was diluted in the same standard diluents buffer of samples. Plates were incubated with detection antibody overnight at 4°C. After washing, plates were incubated with HRP anti-rabbit antibody for 30 min at RT, then they were washed and stabilized chromogen was added in each well for 20 min in a dark chamber at RT. After stopping the reaction with 2N H_2SO_4, the absorbance of plates was read at 450 nm using the Multiskan® spectrum spectrophotometer. The standard curves were established using a variety of concentrations (15.63–1,000 pg/ml) of a synthetic Aβ42 peptide. Data were expressed as µg of Aβ42/g of wet tissue.

2.6. Statistical analysis

For imaging and autoradiographic studies results are expressed as means ± SEM. To compare the two groups of mice (Tg versus WT), a Mann-Whitney test was used. For biochemical analysis, results are expressed as means ± SEM. To compare the two groups of mice (Tg versus WT), a Mann-Whitney test was used. Data for multiple variable comparisons were analyzed by a Kruskal-Wallis test with a Dunns multiple comparison test (GraphPad Instat, GraphPad Software, San Diego, CA, USA). The level of significance was $p < 0.05$.

Correlations between two quantitative parameters in 19 months-old mice were estimated by Spearman tests (GraphPad Instat, GraphPad Software, San Diego, CA, USA). The level of significance was $p < 0.05$.

3. Results

3.1. Animals

We observed no physiological problem in any animal, and no difference in body weight was observed between Tg and WT animals at each age (6 months: 41.1 ± 2.2 vs 40.5 ± 1.3 g; 9 months: 44.0 ± 0.9 vs 44.4 ± 1.7 g; 12 months: 43.5 ± 0.6 vs 43.4 ± 2.2 g; 15 months: 45.4 ± 1.3 vs 43.1 ± 2.9 g; 19 months: 43.2 ± 1.0 vs 42.4 ± 2.1 g).

3.2. PET imaging

As shown in Fig.1A, the highest accumulation of [^{18}F]AV-45 was observed in the Tg group at 19 months-of-age. In the cerebellum (Fig.1B), no significant difference in SUV values was observed whatever the age between Tg and WT mice, although a tendency to rise was observed in both groups at 15 and 19 months. In the cortex (Fig.1C), the SUVr to cerebellum was progressively increased from 10% (9 months) to 16% (19 months) in Tg vs WT animals. A significant increase in Tg vs WT was observed at 9 months (1.09 ± 0.02 vs 0.99 ± 0.02, p = 0.0159), 15 months (1.12 ± 0.03 vs 0.99 ± 0.02, p = 0.0159) and 19 months (1.14 ± 0.03 vs 0.98 ± 0.02, p = 0.0079), while no difference was seen at 6 months (1.05 ± 0.04 vs 0.99 ± 0.02, p = 0.3095), and a non-significant increase was observed at 12 months (1.10 ± 0.03 vs 1.00 ± 0.05, p = 0.0556). In the hippocampus (Fig.1D), a significant 14% increase was observed in Tg vs WT animals at 19 months (0.98 ± 0.02 vs 0.86 ± 0.02, p = 0.0159), but not before this age. In the striatum, no difference was observed between groups whatever the age (Fig.1E).

The brain accumulation of [^{18}F]DPA-714 is illustrated in Fig.2A. In the cerebellum (Fig.2B), no significant difference in SUV values was observed whatever the age between Tg and WT mice, although a tendency to rise was observed in both groups at 15 and 19 months. In the cortex (Fig.2C), the SUVr to cerebellum was significantly increased around 20% in Tg vs WT

animals at 12 months (1.05 ± 0.04 vs 0.85 ± 0.05, p = 0.0317) and at 19 months (1.02 ± 0.03 vs 0.82 ± 0.04, p = 0.0159) while the increase was not statistically significant at 15 months (0.99 ± 0.03 vs 0.82 ± 0.05, p = 0.11). In the hippocampus (Fig.2D), a significant 17% increase was observed in Tg vs WT animals at 19 months (0.73 ± 0.01 vs 0.62 ± 0.01, p = 0.0159), but not before this age. In the striatum, no difference was observed between groups whatever the age (Fig.2E).

3.3. Ex vivo studies at 19 months-of-age

3.3.1. β-Amyloid quantification

By using W02 clone to label amyloid peptide (amino acids residues 4-10 of human Aβ), we observed that 19 months-old APPswePS1dE9 mice displayed numerous amyloid deposits in all brain regions studied with a major increase in the temporal cortex. Indeed, the raw integrated density for amyloid deposits was significantly higher in Tg than in WT mice in all brain regions (Fig.3A and 3B).

Aβ42 levels in the temporal cortex, hippocampus, striatum and cerebellum of 19-months old mice have been quantified by ELISA (Table 1). Results showed that these mice had more Aβ42 in the cerebellum than in cortex, hippocampus and striatum (increase in 102, 242 and 228%, respectively to the three brain regions). The rate of Aβ42 in the brain of age-matched WT mice was under the limit of detection.

3.3.2. Neuroinflammatory markers

TSPO: The TSPO density at 19 months was measured by [^{3}H]PK-11195 binding in the 4 regions of interest, i.e. the cortex, hippocampus, striatum and cerebellum as illustrated in Fig.4A. A statistically significant increase was observed between Tg and WT groups in the cortex (26% increase: 9.25 ± 0.34 vs 7.33 ± 0.33 cpm/mm^2, p = 0.0079), hippocampus (37%

increase: 10.72 ± 0.30 vs 7.83 ± 0.27 cpm/mm^2, p = 0.0079) and striatum (38% increase: 7.75 ± 0.25 vs 5.60 ± 0.17 cpm/mm^2, p = 0.0079), while this increase was non significantly different in the cerebellum (16% increase: 10.83 ± 0.94 vs 9.32 ± 0.32 cpm/mm^2, p = 0.0952). We also studied TSPO expression by western blot and immunofluorescence. The immunoreactivity of TSPO was similar in WT and Tg groups in each brain area except in the striatum where TSPO expression was significantly lower than that measured in the cortex both in WT and APPswePS1dE9 mice (16.82 and 10.78 times lower for WT and Tg mice, respectively). In addition, confocal staining also showed that the level of TSPO expression was identical in APPswePS1dE9 and wild-type mice (supplementary file 1).

Pro-inflammatory cytokine levels: Brain quantification of IL-1β, TNF-α and IL-6 levels showed no difference between WT and Tg mice except in striatum where a significant decrease in IL-1β levels was measured (45.6%) in Tg mice compared to WT mice (Table 2). For IL-6, levels were under the limit of detection in the cortex, hippocampus and striatum in both groups. In the cerebellum, IL-6 means showed a large inter-individual variability (8.17 ± 2.31 and 18.87 ± 12.40 pg/mg protein in WT and Tg, respectively).

Microglia: CD68 (Cluster of Differentiation 68) called "macrosialin" in mouse corresponding to a macrophage-restricted glycoprotein (Holness et al. 1993) and used as a marker of activated microglia with active phagocytosis (Bornemann et al. 2001; Damjanac et al. 2007). APPswePS1dE9 mice displayed many CD68-positive cells that develop many extensions in the cortex, hippocampus and striatum whereas in WT mice the staining remained confined to small microglia with no or very short extensions (Fig.5A). The raw integrated density of CD68 was 5.6, 1.8 and 2.3-fold higher in the cortex, hippocampus and striatum of APPswePS1dE9, respectively compared to WT mice (Fig.5B). However, in the cerebellum

the CD68 staining was more present in blood vessels in both mice groups and no difference was observed (Fig.5A and 5B).

Astrocytes: In the cortex, hippocampus and striatum, the immunoreactivity of GFAP increased in Tg versus WT mice (243.6%, 60.8% and 292.7%, respectively) while GFAP levels were similar in cerebellum (Fig. 7A).

These results were confirmed by confocal immunostaining where the density of astrocytes (GFAP-positive cells) was 17.3, 2.3 and 8.3-fold higher in the cortex, hippocampus and striatum of APPswePS1dE9 compared to respective brain regions of WT mice (Fig.6B and 6C). Astrocytes had a larger cell body with a strong GFAP-positive signal and a stellar morphology characteristic under gliosis. No significant increase was noted in the cerebellum between two groups (Fig.6B and 6C).

3.4. Correlations between in vivo and ex vivo parameter values at 19 months

The rho and p values measured using the Spearman test are shown in supplementary file 2.

First, in vivo we showed that the amyloid burden assessed by [^{18}F]AV-45 SUVr values in the cortex and hippocampus were strongly and positively correlated with the TSPO imaging assessed by [^{18}F]DPA-714 (Table 1). No correlation was observed before 19 months. Significant positive correlations in the cortex and hippocampus were also observed between [^{18}F]AV-45 SUVr values and *ex vivo* W02 (Table 2). In addition, the amyloid burden was also found to be positively correlated with the inflammatory component. Indeed, in the cortex and hippocampus, [^{18}F]AV-45 SUVr values were correlated with GFAP and CD68 raw integrated density as well as with [^{3}H]PK-11195 binding values (Table 2). No correlation was reported in the striatum whatever the *ex vivo* parameter tested (Tables 1 and 2). Furthermore, amyloid burden quantified with W02 staining was also positively correlated with [^{18}F]DPA-714 SUVr

values, [^{3}H]PK-11195 binding, GFAP and CD68 raw integrated density in the cortex and hippocampus (Tables 3 to 5).

Secondly, for inflammatory component, [^{18}F]DPA-714 SUVr values were positively correlated with [^{3}H]PK-11195 binding values in the cortex and hippocampus (Table 3). In addition, [^{18}F]DPA-714 SUVr values and [^{3}H]PK-11195 binding values were strongly and positively correlated with CD68 in all tested areas (Table 3 and 4). In vivo and ex vivo TSPO values were also correlated with GFAP density value in all areas except in the cortex and striatum for *in vivo* TSPO (Tables 3 and 4).

4. Discussion

Several studies have examined the role of the inflammatory component in AD by investigating its impact on amyloidogenesis and neuronal death. Indeed, it is well known that the β-amyloid peptide (Aβ) leads to an inflammatory response orchestrated by microglia and inflammatory factors in turn able to activate the β- and γ-secretases, which cleave the amyloid precursor protein (APP) to Aβ (Liu and Chan 2014; Heneka et al. 2010). However, a longitudinal follow-up of both amyloid load and neuroinflammation in the same animals had never been studied. In the present study, we explored these two components in a transgenic mouse model Alzheimer APPswePS1dE9 largely used in AD research, from 6 to 19 months-of-age. In addition, we studied the neuroinflammatory and neuroanatomical status of brain's mice at 19 months.

Quantitative analysis of PET data from either mice or rats brain are severely affected by partial volume effect (PVE). It has been recently shown that PVE improved quantification of the PET signal in cerebral imaging of mice (Brendel et al. 2014). In this study, we applied the Reblurred Van Cittert algorithm to correct for PVE (Carasso 1999), which makes no

assumption about the homogeneity of regional uptake and does not require any anatomical information.

Using this analysis method for the longitudinal follow-up of APPswePS1dE9 mice with the β-amyloid PET tracer [^{18}F]AV-45, we observed that the more affected region was the cortex with a significantly increased signal from 9 months-of-age compared to age-matched WT animals. In this model, very limited β-amyloid deposits were detected in vitro by thioflavine and the anti-body 3D6 as early as 4 months-of-age in the cortex and hippocampus, these deposits being more visible from 6 months (Garcia-Alloza et al. 2006). Previous findings showed that no accumulation of the PET tracer [^{11}C]PIB nor increase in the cortex to cerebellum ratio was detected in vivo in these Tg mice at different ages (9 to 19 months), whereas this was the case in other Tg models with amyloid deposits such as APP23 (Maeda et al. 2007; Snellman et al. 2012) and APP/PS1 (Manook et al. 2012). The differences in Aβ plaque structure and deposition between animal models of AD could explain these differences obtained with the same tracer. Our study indicates that [^{18}F]AV-45 seems more sensitive than [^{11}C]PIB for detection of plaques in the APPswePS1dE9 model, as our results are in agreement with in vitro data. In still another Tg model of AD, i.e. APP/PS1-21, [^{18}F]AV-45 was also able to accumulate in the cortex and hippocampus at 8 and 12 months-of-age (Poisnel et al. 2012). Another fluorinated tracer of plaques, [^{18}F]-florbetaben, had an increased cortical accumulation from 13 months in the APP-Swe model (Rominger et al. 2013). Our study demonstrated therefore the usefulness of PET imaging using [^{18}F]AV-45 in the APPswePS1dE9 model, that could be of immense value for in vivo monitoring of potential treatments aimed at reducing the amyloid deposits.

A number of evidence indicates that neuroinflammation is associated with AD, involving microglia activation and astrogliosis (Glass et al. 2010 for review). The TSPO, a five transmembrane protein localized in the outer mitochondrial membrane, is expressed in

microglia and astrocytes, its overexpression being related to the activation of these cell populations, and is therefore considered as a biomarker of neuroinflammation (Papadopoulos et al. 2006; Chen and Guilarte 2008). In the aim to explore this process in vivo, a number of PET tracers of TSPO were developed in recent years as an alternative to the reference ligand [^{11}C]PK-11195 (Dollé et al. 2009). In AD, clinical studies have found no detection (Varrone et al. 2013) or increase of TSPO density (Kreisl et al. 2013, Schuitemakeret al. 2013), using different PET tracers including [^{18}F]FEDAA1106, [^{11}C]PBR-28 and [^{11}C]PK-11195. Another recent tracer, [^{18}F]DPA-714, has already been used in a number of preclinical rodent models of brain diseases such as glioma (Winkeler et al. 2012), multiple sclerosis (Abourbeh et al. 2012), cerebral ischemia (Martin et al. 2010; Boutin et al. 2013), traumatic brain injury (Wang et al. 2014) and epilepsy (Harhausen et al. 2013), and has begun to be used in clinical studies (Corcia et al. 2012) although no data are to date available in AD.

The analysis of dynamic PET studies with [^{18}F]DPA-714 requires the definition of a reference region when no arterial sampling is available. Currently, the method of choice consists in a clustering approach called Supervised Cluster Analysis (SVCA), in which the PET voxels are segmented based on difference in time-activity curves (Turkheimer et al. 2007, Yaqub et al. 2012). While this approach has been developed and used with [^{11}C]PK11195, it has not yet been defined and validated for [^{18}F]DPA714. An alternative approach consists in calculating a standard uptake value ratio (SUVr) using the cerebellum as reference region. While less precise than SVCA, such approach has been used previously with [^{18}F]DPA-714 (Winkeler et al. 2012) and with [^{11}C]PK11195 (Versijpt et al. 2003, Kropholler et al. 2007). In this study, we used a SUVr approach as semi-quantitative index for PET image analysis, and observed an increased accumulation of [^{18}F]DPA-714 in the cortex of Tg mice compared to age-matched WT from 12 months-of-age and in the hippocampus at 19 months. This result is in agreement

with previous data obtained in this same animal model using [^{11}C]PK-11195 (Venneti et al. 2009).

Our multitracer PET study in same animals at different ages demonstrated that in these experimental conditions, the cortex was the brain region affected earliest by the occurrence of β-amyloid plaques and rising in TSPO density, the second region being the hippocampus, whereas no significant effect was visible in the striatum. Although the sensitivity in the detection of the plaques and TSPO by their respective tracer, [^{18}F]AV-45 and [^{18}F]DPA-714, may be confounding, our imaging results indicate that neuroinflammation progresses concomitantly with increased amyloid burden. For the first time, *in vivo* longitudinal monitoring can detect at 9 and 12 months, amyloid plaques and inflammation in the cortex, respectively, although an increase in the BBB permeability has been described from 14 months in this model (Minogue et al. 2014). Even though this study provides valuable information on longitudinal progression, it has some limitations. In particular, the sample sizes were limited which lowered the statistical power of the tests and increased the variability of the measured responses.

Several *ex vivo* data revealed that multiple inflammatory indexes (number of astrocytes, microglia, cytokine levels…) significantly correlated with soluble Aβ level, rather than amyloid plaque burden or insoluble Aβ level, in female APPswePS1dE9 mice at the age of 3.5, 6, and 12 months (Zhang et al. 2012). This thorough analysis of inflammatory changes in APPswePS1dE9 mice indicated that inflammatory responses might occur early at the pre-plaque stage of the disease, and were strongly enhanced at the plaque-stage of the disease, providing further evidence to support the emerging notion that inflammatory response is an early event in AD (Zhang et al. 2012).

We examined more extensively the relationships between these processes, i.e β-amyloid load and neuroinflammation, through different complementary approaches in the brain of our mice after the last in vivo scan, at 19 months-of-age.

The study of β-amyloid by immunohistochemistry showed that at this advanced stage of the disease, the more affected brain region was the cortex followed by the hippocampus, the striatum and the cerebellum, in agreement with our imaging results. It is difficult to compare our results to literature data because many reports showed amyloid load in cortex and hippocampus of these mice only at 12 months of age (Izco et al. 2014; Zhang et al. 2012; Ruan et al. 2009; Garcia-Alloza et al. 2006). In addition, amyloid deposits were detected by different antibodies against specific amyloid peptides or not (Aβ42, Aβ40) or dyes such as thioflavin S which binds to amyloid fibrils. However, Liu et al. (2008) showed an increase in the Aβ deposits (clone 4G8 which is now replaced by clone W02) in the cortex and hippocampus of 18-month-old APPswePS1dE9 mice and also few Aβ deposits were observed in the cerebellum. Recently, BF-168-positive Aβ plaques (BF-168 specifically binds to Aβ) in the cerebellum were also shown at 8, 12 and 18 months of age but there are less BF-168-positive Aβ plaques in the cerebellum than in the frontal cortex (Kuwabara et al. 2014). Contrary to other studies, we quantified total Aβ42 (by using guanidine for extraction) in each brain area and not in whole brain as previously published (Izco et al. 2014; Zhang et al. 2012; Garcia-Alloza et al. 2006). Here, we showed for the first time in these Tg mice that the levels of total Aβ42 were higher in the cerebellum than in other areas at 19 months of age. ELISA analyses of the levels of total Aβ1-42 peptides in different brain regions of 12-month-old Tg mice also showed higher levels in the cerebellum than in frontal cortex, hippocampus and striatum (Xiong et al. 2011). Recently, it has been shown that there are high levels of soluble Aβ1-42 by ELISA in the cerebellum of APPswePS1dE9 mice at 3 and 6 months (Kuwabara et al. 2014). In AD patients, it is well known that Aβ plaque formation occurs in the cerebral

cortex and hippocampus, whereas only a diffuse type of Aβ accumulation was observed in the cerebellum (Braak et al. 1989; Mann et al. 1996). In addition to Aβ accumulation, previous studies showed that the levels of Aβ1–42 in the cerebellum increased more than twofold in AD patients relative to controls (Hashimoto et al. 2010).

It can be noted that, as thioflavine, tracers used in clinical and animal studies, such as [^{18}F]AV-45, bind exclusively to aggregated Aβ (Choi et al. 2009). This could explain the differences we observed in the localization and density of Aβ that we measured through different methods (imaging, immunohistochemistry, ELISA).

At 19 months-old APPswePS1dE9 mice, the density of TSPO measured by quantitative autoradiography with [^{3}H]PK-11195 showed an increase in all brain regions studied, i.e. the cortex, hippocampus, striatum and in a lesser extend cerebellum. These *in vitro* data are also coherent with our imaging experiments aimed at exploring the same molecular target, TSPO, but probably with less sensitivity, thus explaining that no significant effect was observed in the striatum. However, the [^{18}F]DPA-714 SUVr values were strongly and positively correlated with those of [^{3}H]PK-11195 binding values in the cortex and hippocampus. For western blot and immunohistochemistry, we used the antibody purchased from Novus which is a monoclonal rabbit antibody produced against a synthetic peptide corresponding to residues in C-terminus of human TSPO (EPR5384 clone). In these experimental conditions, no difference was observed between Tg and age-matched WT mice. To our knowledge, no study using this monoclonal TSPO antibody is reported in the literature. Recently, the 3D structure of mitochondrial TSPO in complex with its high-affinity ligand PK-11195 was described and indicated that a tight bundle of five transmembrane α helices form a hydrophobic pocket accepted ligand (Jaremko et al. 2014). Furthermore, the C-terminal is highly positively charged and exposed to the cytoplasm. It might be assumed that the binding of the antibody to the C-terminus of TSPO is not stable and limits its fixation during

immunostaining. Other studies indicated differences between the binding sites of radioligands and histochemical antibodies (Cosenza-Nashat et al., 2009; Kuhlmann et al., 2000; Banati, 2002).

Besides this molecular marker of inflammation, we also studied cytokine production at this advanced age of disease. Results showed no difference between Tg and WT mice except in striatum where levels decreased in Tg mice. Perhaps, this decrease could be due to alteration of this brain area observed from 12 months in this Tg mouse model (Richner et al. 2009). Again, the comparison with the literature is very limited because most studies have quantified the levels of IL-1β, TNF-α and IL-6 by ELISA in total brain or were only interested by mRNA levels and no information after 12-months of age (Zhang et al. 2012; Minogue et al. 2014) or made immunostaining of these factors (Ruan et al. 2009). While mRNA expression increased in hippocampus of 14- and 24-month-old APPswePS1dE9 mice (Minogue et al. 2014), no increase of protein production was observed in 19-month-old Tg versus WT mice. In previous studies, no difference of TNF-α and IL-6 production was observed in 18-month-old Tg versus WT mice (Couturier et al. 2012). At this advanced stage of the disease, these cytokines would not be the most relevant markers of inflammation. It is well known that aging also induced cytokine production (Orre et al. 2014; Kumagai et al. 2007).

In this study, we also stained microglia and astrocytes by CD68, a lysosomal protein that is upregulated in phagocytic cells (Zotova et al. 2011) and GFAP, respectively. For microglia, other markers such as isolectine B4, CD11b, Iba1 are used but results are in accordance and showed a gradually increase of the number of microglia in cortex and hippocampus of these Tg mice (Izco et al. 2014; Minogue et al. 2014; Ruan et al. 2009; Zhang et al. 2012). Here, immunoreactivity of CD68 was significantly increased in cortex, hippocampus and striatum of Tg mice compared with WT mice as it was observed for CD68 mRNA in 14- and 24-month-old APPswePS1dE9 mice (Minogue et al. 2014). Surprisingly, no difference was

observed in the cerebellum unlike the amyloid burden. Recently, it was shown that there are less Iba1-positive cells per plaques in cerebellum than in cortex and hippocampus at 18 months of age (Kuwabara et al. 2014). For GFAP, western blot and immunostaining gave similar results with significant increase in its expression in cortex, hippocampus and striatum of Tg compared to WT mice. These results are in accordance with previous data from 6 to 18 months of age (Ruan et al. 2009; Zhang et al. 2012; Kuwabara et al. 2014). As for microglia, no modification of GFAP expression in the cerebellum was observed between Tg and WT mice at 19 months of age. Kuwabara et al. (2014) also showed no reactive astrocytes in the cerebellar molecular layer of 18-month-old APPswePS1dE9 mice. In the cerebellum of these Tg mice, at a very advanced stage of the disease, the presence of amyloid deposits observed showed no inflammatory response compared to WT mice but extensive research on the inflammatory component in the cerebellum is needed to better understand the chronology of amyloid deposits and the inflammatory response in this area.

Interestingly, correlations analyses between amyloid load and inflammation showed that PET imaging data ([^{18}F]AV-45 and [^{18}F]DPA-714) were not only positively correlated, but also with *ex vivo* data (W02, GFAP, CD68, [^{3}H]PK-11195) at 19 months, indicating the usefulness of PET imaging for these impairments and enhancing the reciprocity between the presence of amyloid deposits and inflammatory response at this advanced stage of disease.

5. Conclusion

In the present study, four highlights are noted: 1) We undertook the first longitudinal imaging study for both inflammation and amyloid load in a well-recognized model of AD, APPswePS1dE9 mice; 2) We showed that in this model the increase in TSPO binding was assessed both using in vivo (imaging) and ex vivo (autoradiographic) approaches. No binding of TSPO was observed in cerebellum while immunostaining of amyloid peptide revealed W0-

2-positive plaques in this region. We can propose that these amyloid deposits in cerebellum seemed not be a stimulator of inflammation, as we observed no significant difference staining of microglia and astrocytes between Tg and WT mice in this region; 3) It seems that at this advanced stage of disease, immunoreactivity of microglia and astrocytes in the cortex, hippocampus and striatum are more relevant to define inflammatory status compared to classical cytokine IL-1β, TNF-α and IL-6. It could be interesting to know the cytokine signature with age of the disease; 4) Interestingly, PET imaging data were not only strongly and positively correlated in the cortex and hippocampus but also with *ex vivo* data of amyloid load and inflammation, highlighting the usefulness of PET imaging and the vicious circle between the amyloid load and inflammation at an advanced stage of disease. The latter may support the interests of anti-amyloid and anti-inflammatory combination therapy.

6. Acknowledgements

The research leading to these results has received funding from the European Union's Seventh Framework Programme (FP7/2007-2013) under grant agreement n°278850 (INMiND) and from Labex IRON (ANR-11-LABX-18-01).

We thank the Laboratoires Cyclopharma for providing fluor-18, and Damien Chassaing and Sylvie Bodard for technical assistance.

Disclosure statement

The authors declare that they have no conflict of interest.

7. References

Abourbeh G, Thézé B, Maroy R, Dubois A, Brulon V, Fontyn Y, et al. Imaging microglia/macrophage activation in spinal cords of experimental autoimmune

encephalomyelitis rats by positron emission tomography using the mitochondrial 18 kDa translocator protein radioligand [^{18}F]DPA-714. J Neurosci 2012;32:5728-36.

Akiyama H, Barger S, Barnum S, Bradt B, Bauer J, Cole GM, et al. Inflammation and Alzheimer's disease. Neurobiol Aging 2000;21:383-421.

Banati RB. Visualizing microglial activation in vivo. Glia. 2002; 40:206–217

Bornemann KD, Wiederhold KH, Pauli C, Ermini F, Stalder M, Schnell L, et al. Abeta-induced inflammatory processes in microglia cells of APP23 transgenic mice. Am J Pathol 2001;158:63-73.

Boutin H, Prenant C, Maroy R, Galea J, Greehalgh AD, Smigova A, et al. [^{18}F]DPA-714: direct comparison with [^{11}C]PK11195 in a model of cerebral ischemia in rats. PLoS One 2013;8:e56441.

Braak H1, Braak E, Bohl J, Lang W. Alzheimer's disease: amyloid plaques in the cerebellum. J Neurol Sci. 1989;93:277-87.

Braak HI, Braak E. Neuropathological stageing of Alzheimer-related changes. Acta Neuropathol 1991;82:239-59.

Brendel M, Delker A, Rötzer C, Böning G, Carlsen J, Cyran C et al. Impact of partial volume effect correction on cerebral β-amyloid imaging in APP-Swe mice using [^{18}F]-florbetaben PET. NeuroImage 2014;84:843-53.

Camus V, Payoux P, Barre L, Desgrandes B, Voisin T, Tauber C, et al. Using PET with 18F-AV45 (Florbetapir) to quantify brain amyloid load in a clinical environment. Eur J Nucl Med Mol Imaging 2012;39:621-31.

Carasso A. Linear and nonlinear image deblurring: a documented study. SIAM J. Numer. Anal. 1999: 36:1659–89.

Chauveau F, Van Camp N, Dollé F, Kuhnast B, Hinnen F, Damont A, et al. Comparative evaluation of the translocator protein radioligands 11C-DPA-713, 18F-DPA-714, and 11C-PK11195 in a rat model of acute neuroinflammation. J Nucl Med 2009; 50:468-76.

Chen MK, Guilarte TR. Translocator protein 18 kDa (TSPO): molecular sensor of brain injury and repair. Pharmacol Ther 2008;118:1-17.

Choi R, Golding G, Zhuang Z, Zhang W, Lim N, Hefti F, et al. Preclinical properties of 18F-AV-45: a PET agent for Aβ plaques in the brain. J Nucl Med 2009; 50:1887-94.

Clark CM, Schneider JA, Bedell BJ, Beach TG, Bilker WB, Mintun MA, et al. Use of florbetapir-PET for imaging beta-amyloid pathology. JAMA 2011;305:275-83.

Corcia P, Tauber C, Vercouillie J, Arlicot N, Prunier C, Praline J, et al. Molecular imaging of microglial activation in amyotrophic lateral sclerosis. PLoS One 2012;7:e52941.

Cosenza-Nashat M1, Zhao ML, Suh HS, Morgan J, Natividad R, Morgello S, Lee SC. Expression of the translocator protein of 18 kDa by microglia, macrophages and astrocytes

based on immunohistochemical localization in abnormal human brain. Neuropathol Appl Neurobiol. 2009;35:306-28.

Couturier J, Paccalin M, Lafay-Chebassier C, Chalon S, Ingrand I, Pinguet J, et al. Pharmacological inhibition of PKR in APPswePS1dE9 mice transiently prevents inflammation at 12 months of age but increases Aβ42 levels in the late stages of the Alzheimer's disease. Curr Alzheimer Res 2012; 9:344-60.

Damjanac M, Rioux Bilan A, Barrier L, Pontcharraud R, Anne C, Hugon J, Page G. Fluoro-Jade B staining as useful tool to identify activated microglia and astrocytes in a mouse transgenic model of Alzheimer's disease. Brain Res 2007;1128:40-9.

Dollé F, Luus C, Reynolds A, Kassiou M. Radiolabelled molecules for imaging the translocator protein (18kDa) using Positron Emission tomography. Curr Med Chem 2009;16:2899-2923.

Fleisher, AS, Chen K, Liu X, Roontiva A, Thiyyagura P, Ayutyanont N, et al. Using Positron Emission Tomography and Florbetapir F18 to image cortical amyloid in patients with mild cognitive impairment or dementia due to Alzheimer disease. Arch Neurol 2011;68:1404-11.

Franklin KBJ, Paxinos, G The mouse brain in stereotaxic coordinates, Third compact edition, Academic Press, New York 2008.

Garcia-Alloza M, Robbins EM, Zhang-Nunes SX, Purcell SM, Betensky RA, Raju S, et al. Characterization of amyloid deposition in the APPswe/PS1dE9 mouse model of Alzheimer disease. Neurobiol Dis 2006;24:516-24.

Glass CK, Saijo K, Winner B, Marchetto MC, Gage FH. Mechanisms underlying inflammation in neurodegeneration. Cell 2010;140:918-34.

Harhausen D, Sudmann V, Khojasteh U, Müller J, Zille M, Graham K, et al. Specific imaging of inflammation with the 18 kDa translocator protein ligand DPA-714 in animal models of epilepsy and stroke. PLoS One 2013;8:e69529.

Hashimoto M1, Bogdanovic N, Volkmann I, Aoki M, Winblad B, Tjernberg LO. Analysis of microdissected human neurons by a sensitive ELISA reveals a correlation between elevated intracellular concentrations of Abeta42 and Alzheimer's disease neuropathology. Acta Neuropathol. 2010;119:543-54.

Heneka MT1, O'Banion MK, Terwel D, Kummer MP. Neuroinflammatory processes in Alzheimer's disease. J Neural Transm. 2010;117:919-47.

Holness CL, da Silva RP, Fawcett J, Gordon S, Simmons DL. Macrosialin, a mouse macrophage-restricted glycoprotein, is a member of the lamp/lgp family. J Biol Chem 1993;268:9661-6.

Izco M, Martínez P, Corrales A, Fandos N, García S, Insua D, et al. Changes in the brain and plasma Aβ peptide levels with age and its relationship with cognitive impairment in the APPswe/PS1dE9 mouse model of Alzheimer's disease. Neuroscience. 2014;263:269-79.

James ML, Fulton RR, Vercouillie J, Henderson DJ, Garreau L, Chalon S, et al. DPA-714, a new translocator protein-specific ligand: synthesis, radiofluorination, and pharmacologic characterization. J Nucl Med 2008 ;49:814–22.

Jankowski JL, Fadale DJ, Anderson J, Xu GM, Gonzales V, Jenkin NA, et al. Mutant preselinins specifically elevate the levels of the 42 residue [beta]-amyloid peptide in vivo: evidence for augmentation of a 42- specific [gamma] secretase. Hum Mol Genet 2004 ;13: 159-70.

Jaremko L, Jaremko M, Giller K, Becker S, Zweckstetter M. Structure of the mitochondrial translocator protein in complex with a diagnostic ligand. Science. 2014;343:1363-6.

Joshi AD, Pontecorvo MJ, Clark CM, Carpenter AP, Jennings DL, Sadowsky CH, et al., and the Florbetapir F18 Study investigators. Performance characteristics of amyloid PET with florbetapir F18 in patients with Alzheimer’s disease and cognitively normal subjects. J Nucl Med 2012;53:378-84.

Klunk WE, Engler H, Nordberg A, Wang Y, Blomqvist G, Holt DP, et al. Imaging brain amyloid in Alzheimer's disease with Pittsburgh Compound-B. Ann Neurol 2004:55:306-19.

Kreisl WC, Lyoo CH, McGwier M, Snow J, Jenko KJ, Kimura N, et al. In vivo radioligand binding to translocator protein correlates with severity of Alzheimer’s disease. Brain 2013;136:2228-38.

Kreutzberg GW. Microglia: a sensor for pathological events in the CNS. Trends Neurosci 1996;19:312-18.

Kropholler MA, Boellaard R, Berckel BN, Schuitemaker A, Kloet RW, Lubberink MJ, et al. Evaluation of reference regions for (R)-[(11)C]PK11195 studies in Alzheimer's disease and mild cognitive impairment. J Cereb Blood Flow Metab 2007;27(12):1965–74.

Kuhlmann AC, Guilarte TR. Cellular and subcellular localization of peripheral benzodiazepine receptors after trimethyltin neurotoxicity. J Neurochem. 2000; 74:1694–1704.

Kumagai N, Chiba Y, Hosono M, Fujii M, Kawamura N, Keino H, Yoshikawa K, Ishii S, Saitoh Y, Satoh M, Shimada A, Hosokawa M. Involvement of pro-inflammatory cytokines and microglia in an age-associated neurodegeneration model, the SAMP10 mouse. Brain Res 2007;1185:75-85.

Kuwabara Y1, Ishizeki M, Watamura N, Toba J, Yoshii A, Inoue T, Ohshima T. Impairments of long-term depression induction and motor coordination precede Aβ accumulation in the cerebellum of APPswe/PS1dE9 double transgenic mice. J Neurochem. 2014. doi: 10.1111/jnc.12728. [Epub ahead of print].

Liu Y, Yoo MJ, Savonenko A, Stirling W, Price DL, Borchelt DR, et al. Amyloid pathology is associated with progressive monoaminergic neurodegeneration in a transgenic mouse model of Alzheimer's disease. Neurobiol Dis 2008;28:13805-14.

Liu Y, Zhu L, Plössl K, Choi SR, Qiao H, Sun X, et al. Optimization of automated radiosynthesis of [18F]AV-45: a new PET imaging agent for Alzheimer's disease. Nucl Med Biol 2010;37:917–25.

Liu L, Chan C. The role of inflammasome in Alzheimer's disease. Ageing Res Rev. 2014;15C:6-15.

Maeda J, Ji B, Irie T, Tomiyama T, Maruyama M, Okauchi T, et al. Longitudinal, quantitative assessment of amyloid, neuroinflammation, and anti-amyloid treatment in a living mouse model of Alzheimer's disease enabled by positron emission tomography. J Neurosci 2007; 27: 10957-68.

Mann DM1, Iwatsubo T, Snowden JS. Atypical amyloid (A beta) deposition in the cerebellum in Alzheimer's disease: an immunohistochemical study using end-specific A beta monoclonal antibodies. Acta Neuropathol. 1996;91:647-53.

Manook A, Yousefi BH, Willuweit A, Platzer S, Reder S, Voss A, et al. Small-animal PET imaging of amyloid-beta plaques with [^{11}C]PIB and its multi-modal validation in an APP/PS1 mouse model of Alzheimer's disease. PLoS ONE 2012;7:e31310.

Martin A, Boisgard R, Thézé B, Van camp N, Kuhnast B, Damont A et al. Evaluation of the PBR/TSPO radioligand [(18)F]DPA-714 in a rat model of focal cerebral ischemia. J Cerb Bloof Flow Metab 2010;30:230-41.

Minogue AM, Jones RS, Kelly RJ, McDonald CL, Connor TJ, Lynch MA. Age-associated dysregulation of microglial activation is coupled with enhanced blood-brain barrier permeability and pathology in APP/PS1 mice. Neurobiol Aging. 2014;35:1442-52.

Mirrione MM, Schiffer WK, Fowler JS, Alexoff DL, Dewey SL, Tsirka SE. A novel approach for imaging brain-behavior relationships in mice reveals unexpected metabolic patterns during seizures in the absence of tissue plasminogen activator. Neuroimage 2007;38(1):34-42.

O'Leary TP, Brown RE. Visuo-spatial learning and memory deficits on the Barnes maze in the 16-month-old APPswe/PS1dE9 mouse model of Alzheimer's disease. Behav Brain Res 2009;201:120-7.

Orre M1, Kamphuis W, Osborn LM, Melief J, Kooijman L, Huitinga I, Klooster J, Bossers K, Hol EM. Acute isolation and transcriptome characterization of cortical astrocytes and microglia from young and aged mice. Neurobiol Aging. 2014;35:1-14.

Papadopoulos V, Baraldi M, Guilarte TR et al. Translocator protein (18 kDa): new nomenclature for the peripheral-type benzodiazepine receptor based on its structure and molecular function. Trends in Pharmacological Sciences 2006;27:402-9.

Poisnel G, Dhilly M, Moustié O, Delamare J, Abbas A, Guilloteau D, Barré L. PET imaging with [18F]AV-45 in an APP/PS1-21 murine model of amyloid plaque deposition. Neurobiol. Aging 2012;33:2561-71.

Richner M, Bach G, West MJ. Over expression of amyloid beta-protein reduces the number of neurons in the striatum of APPswe/PS1DeltaE9. Brain Res. 2009;1266:87-92.

Rominger A, Brendel M, Burgold S, Keppler K, Baumann K, Xiong G, et al. Longitudinal assessment of cerebral β-amyloid deposition in mice overexpressing Swedish mutant β-amyloid precursor protein using 18F-florbetaben PET. J Nucl Med 2013;54:1127-34.

Rosenberg PB, Wong DF, Edell SL, Ross JS, Joshi AD, Brasic JR, et al. Cognition and amyloid load in Alzheimer disease imaged with florbetapir F18 (AV-45) positron emission tomography. Am J Geriatr Psychiatry 2013;21:272-8.

Ruan L, Kang Z, Pei G, Le Y. Amyloid deposition and inflammation in APPswe/PS1dE9 mouse model of Alzheimer's disease. Curr Alzheimer Res 2009 ;6:531-40.

Savonenko A1, Xu GM, Melnikova T, Morton JL, Gonzales V, Wong MP, et al. Episodic-like memory deficits in the APPswe/PS1dE9 mouse model of Alzheimer's disease: relationships to beta-amyloid deposition and neurotransmitter abnormalities. Neurobiol Dis 2005;18:602-17.

Schuitemaker A, Kropholler MA, Boellaard R, Van de Flier WM, Kloet RW, Van der Doef TF, et al. Microgial activation in Alzheimer's disease: an (*R*)-[^{11}C]PK11195 positron emission tomography study. Neurobiol Aging 2013;34:128-36.

Snellman A, Lopez-Picon FR, Rokka J, Escola O, Wilson I, Farrar G, et al. Pharmacokinetics of [18F]flutemetamol in wild-type rodents and its binding to beta amyloid deposits in a mouse model of Alzheimer's disease. Eur J Nucl Med Mol Imaging 2012;39:1784-95.

Turkheimer FE, Edison P, Pavese N, Roncaroli F, Anderson AN, Hammers A, Gerhard A, Hinz R, Tai YF, Brooks DJ. Reference and target region modeling of [11C]-(R)-PK11195 brain studies. J Nucl Med. 2007;48(1):158-67.

Varrone A, Mattsson P, Forsberg A, Takano A, Nag S, Gulyas B, et al. In vivo imaging of the 18-kDa translocator protein (TSPO) with [^{18}F]FEDAA1106 and PET does not show increased binding in Alzheimer's disease patients. Eur J Nucl Med Mol Imaging 2013;40:921-31.

Venneti S, Lopresti BJ, Wiley CA. The peripheral benzodiazepine receptor (Translocator protein 18kDa) in microglia: from pathology to imaging. Prog Neurobiol 2006; 80:308-22.

Venneti S, Lopresti BJ, Wang G, Hamilton RL, Mathis CA, Klunk WE, et al. PK11195 labels activated microglia in Alzheimer's disease and in vivo in a mouse model using PET. Neurobiol Aging 2009;30:1217-26.

Versijpt JJ, Dumont F, Laere KJ, Decoo D, Santens P, Audenaert K, et al. Assessment of neuroinflammation and microglial activation in Alzheimer's disease with radiolabelled PK11195 and single photon emission computed tomography. A pilot study. Eur Neurol 2003;50(1):39–47.

Wang Y, Yue X, Kieseetter DO, Niu G, Teng G, Chen X. PET imaging of neuroinflammation in a rat traumatic brain injury model with radiolabeled TSPO ligand DPA-714. Eur J Nucl Med Mol Imaging 2014 Mar11.

Winkeler A, Boisgard R, Awde AR, Dubois A, Thézé B, Zheng J, et al. The translocator protein ligans [^{18}F]DPA-714 images glioma and activated microglia in vivo. Eur J Nucl Med Mol Imaging 2012;39:811-23.

Wong DF, Rosenberg PB, Zhou Y, Kumar A, Raymont V, Ravert HT, et al. In vivo imaging of amyloid deposition in Alzheimer disease using the radioligand 18F-AV-45 (florbetapir F 18). J Nucl Med 2010;51: 913-20.

Xiong H1, Callaghan D, Wodzinska J, Xu J, Premyslova M, Liu QY, Connelly J, Zhang W. Biochemical and behavioral characterization of the double transgenic mouse model (APPswe/PS1dE9) of Alzheimer's disease. Neurosci Bull. 2011;27:221-32.

Yaqub M, van Berckel BN, Schuitemaker A, Hinz R, Turkheimer FE, Tomasi G, Lammertsma AA, Boellaard R. Optimization of supervised cluster analysis for extracting reference tissue input curves in (R)-[(11)C]PK11195 brain PET studies. J Cereb Blood Flow Metab. 2012;32(8):1600-8.

Zhang W1, Bai M, Xi Y, Hao J, Zhang Z, Su C, et al. Multiple inflammatory pathways are involved in the development and progression of cognitive deficits in APPswe/PS1dE9 mice. Neurobiol Aging. 2012;33:2661-77.

Zotova E, Holmes C, Johnston D, Neal JW, Nicoll JA, Boche D. Microglial alterations in human Alzheimer’s disease following Abeta42 immunization. Neuropathol Appl Neurobiol 2011; 37:513e524.

8. Figure legends

Fig.1: **PET brain image with [^{18}F]AV-45 in WT and Tg mice according to age.**

Panel A: Representative coronal images in 6-month-old (upper) and 19 month-old (lower) Tg (left) and WT (right) mice. SUV of tracer accumulation in the cerebellum in WT and Tg mice (**Panel B**). SUVr to cerebellum of tracer accumulation in the cortex **(Panel C)**, hippocampus **(Panel D)**, and striatum **(Panel E**) at different ages (6, 9, 12, 15, 19 months). *, $p < 0.05$ compared to WT age-matched mice (Mann-Whitney test).

Fig.2: **PET brain image with [^{18}F]DPA-714 in WT and Tg mice according to age.**

Panel A: Representative coronal images in 6-month-old (upper) and 19 month-old (lower) Tg (left) and WT (right) mice. SUV of tracer accumulation in the cerebellum in WT and Tg mice (**Panel B**). SUVr to cerebellum of tracer accumulation in the cortex **(Panel C)**, hippocampus **(Panel D)**, and striatum **(Panel E**) at different ages (6, 9, 12, 15, 19 months).

*, $p < 0.05$ compared to WT age-matched mice (Mann-Whitney test).

Fig.3: Immunoreactivity of Aβ in 19 months-old WT and Tg mice.

Panel A: Representative confocal images of Aβ (clone W02) (green channel) and DAPI (blue channel) in the cortex, hippocampus, striatum and cerebellum of 19-months old WT and Tg mice. **Panel B:** Integrated density (product of Area and Mean Gray Value) was defined by using Image J software 1.47V. Scatter dot plot was shown and line represented mean. $^{**}p < 0.01$ compared to WT mice (Mann Whitney test). Scale bar: 23 µm.

Fig.4: **Autoradiography of TSPO with [^{3}H]PK11195 in 19 months-old WT and Tg mice**.

Panel A: Representative autoradiographic images obtained on16 µm-thickness sagittal brain sections: total binding in WT (a) and Tg (b) mice; non-specific binding in WT (c) and Tg (d) mice. Four anatomical regions of interest (CO, cortex; HI, hippocampus; ST, striatum; CE, cerebellum) were manually selected and identified according to the Franklin and Paxinos atlas (e, lateral 1.44 mm). **Panel B**: The radioactivity of ROIs was expressed as mean cpm/mm^2 (8 sections were analyzed and subtracted from the non-specific binding by animal) in the four regions of interest. *, $p < 0.05$ compared to WT mice (Mann-Whitney test).

Fig.5: Immunoreactivity of CD68 in 19 months-old WT and Tg mice.

Panel A: representative confocal images of CD68 (red channel) and DAPI (blue channel) in cortex, hippocampus, striatum and cerebellum of 19-months old WT and Tg mice. Scale bar: 23 µm. **Panel B:** Integrated density (product of Area and Mean Gray Value) was defined by using Image J software 1.47V. Scatter dot plot was shown and line represented mean. $^{*}p < 0.05$, $^{**}p < 0.01$ compared to WT mice by a Mann Whitney test. **Panel C:** Magnified image of region of interest surrounded by a white square in Tg or WT image.

Fig.6: Immunoreactivity of GFAP in 19 months-old WT and Tg mice.

Panel A: Representative immunoblots showed the immunoreactivity of GFAP in the cortex (CO), hippocampus (HI), striatum (ST) and cerebellum (CE) of 19-months old WT and APPswePS1dE9 (Tg) mice. Semi-quantitative analysis of immunoblot was performed using Gene Tools software (Syngene, Ozyme France). The immunoreactivity of protein was normalized to β-actin immunoreactivity. The results are expressed as arbitrary units. Results are mean ± SEM for 5 mice in each group. $^{*}p < 0.05$, $^{**}p < 0.01$ compared to WT mice by a Mann Whitney test. **Panel B:** Representative confocal images of GFAP (red channel) and DAPI (blue channel) in cortex, hippocampus, striatum and cerebellum of 19-months old WT

and Tg mice. Scale bar: 23 µm. **Panel C:** Integrated density (product of Area and Mean Gray Value) was defined by using Image J software 1.47V. Scatter dot plot was shown and line represented mean. $^{**}p < 0.01$ compared to WT mice by a Mann Whitney test.

9. Tables

Table 1: Aβ42 levels in the cortex, hippocampus, striatum and cerebellum of APPswePS1dE9

	cortex	hippocampus	striatum	cerebellum
Aβ42 (µg/g tissue)	43.29 ± 8.79	25.46 ± 8.00*	26.48 ± 9.89*	87.04 ± 9.76

After the last imaging studies, 19-months old mice were sacrificed to quantify Aβ42 levels as described in method section. Results are mean ± SEM of 5 Tg mice and expressed in µg/g tissue. *p<0.05 compared to Aβ42 levels in cerebellum after Kruskal-Wallis and a Dunn's post-hoc test.

Table 2: Pro-inflammatory factors in brain of APPswePS1dE9 and WT mice

	IL-1 β		TNF-α	
	WT	Tg	WT	Tg
CO	59.39 ± 8.45	52.86 ± 6.52	1.65 ± 0.78	1.72 ± 0.44
HI	73.03 ± 11.21	74.55 ± 5.97	2.33 ± 0.68	3.36 ± 1.73
ST	**427.10 ± 33.82**	**232.20 ± 25.55***	11.06 ± 3.97	6.93 ± 3.22
CE	110.10 ± 13.49	82.86 ± 13.60	1.35 ± 0.22	3.15 ± 1.93

IL1-β and TNF-α levels measured in 19-months old APPswePS1dE9 (Tg) versus WT mice by ELISA as described in method section. Cytokine levels were expressed in pg/mg protein and are mean ± SEM from 5 mice per group. *p<0.05 compared to striatal IL-1β level in WT mice by a Mann Whitney test.

Figure 1 A

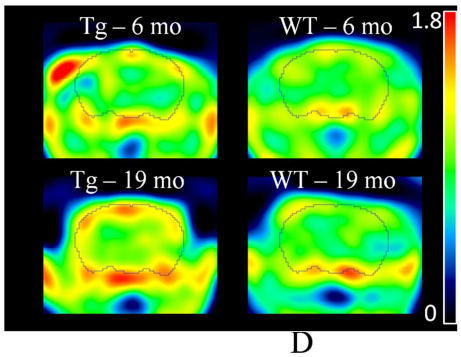

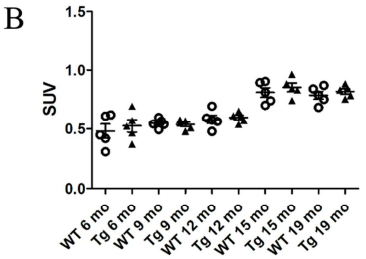

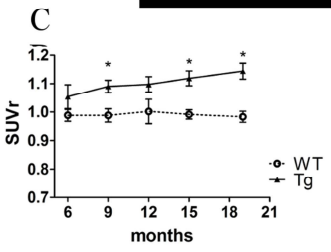

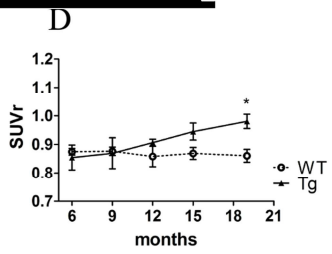

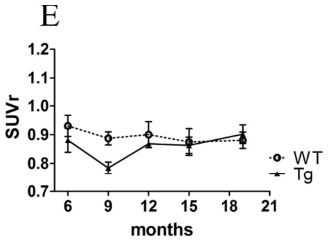

Figure 2 A

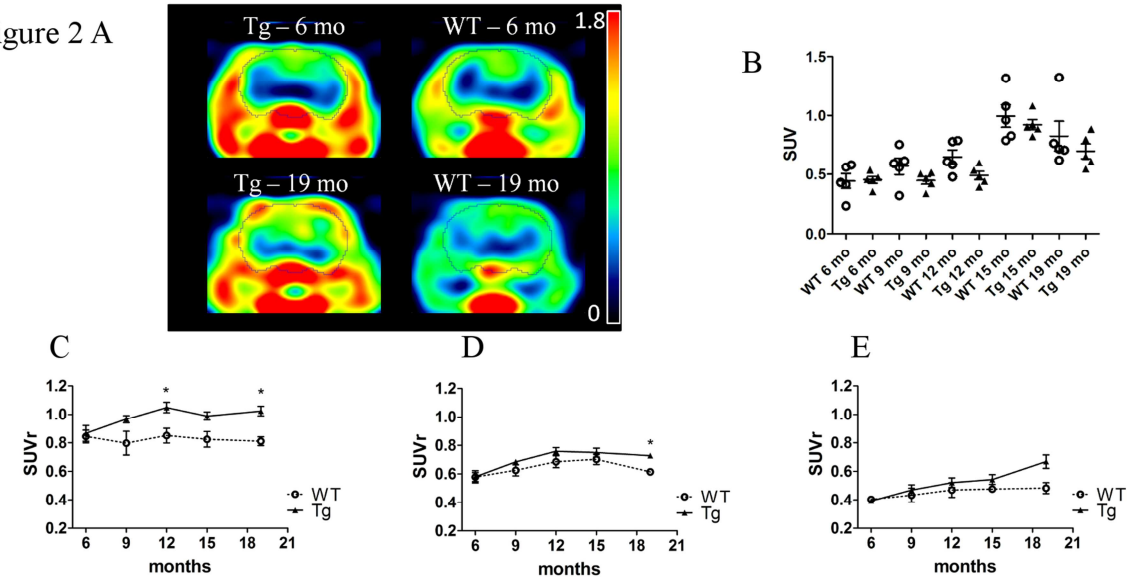

Figure 3

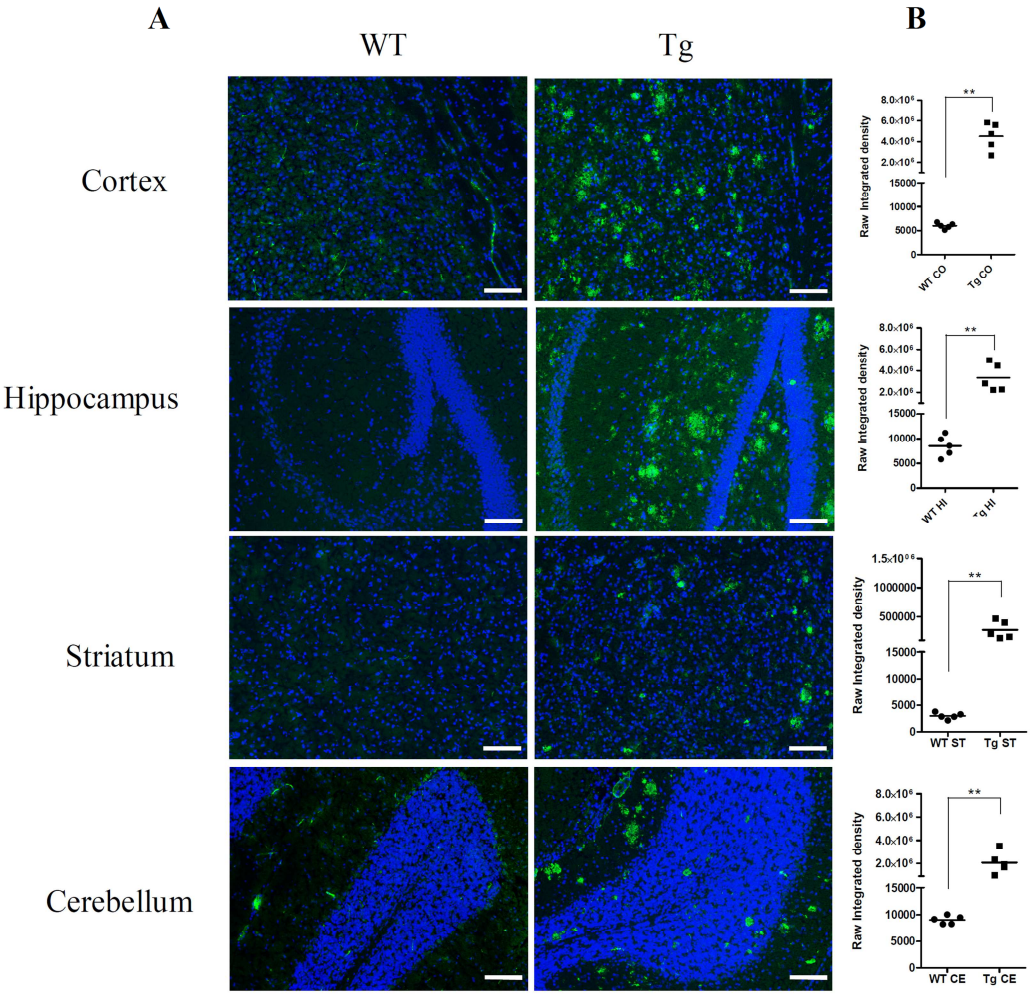
A
WT
Tg
B
Cortex
Hippocampus
Striatum
Cerebellum
Raw Integrated density
WT CO
Tg CO
WT HI
Tg HI
WT ST
Tg ST
WT CE
Tg CE
**

Figure 4 A

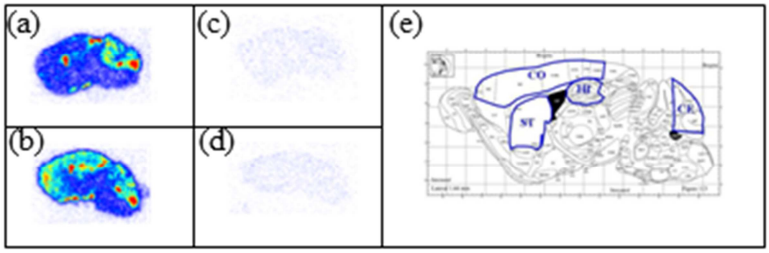

B

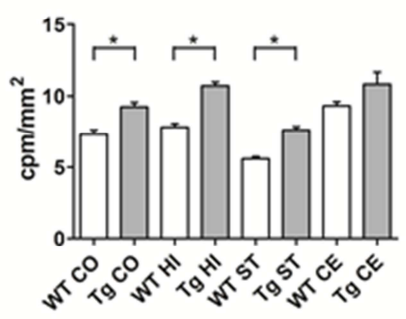

Figure 5

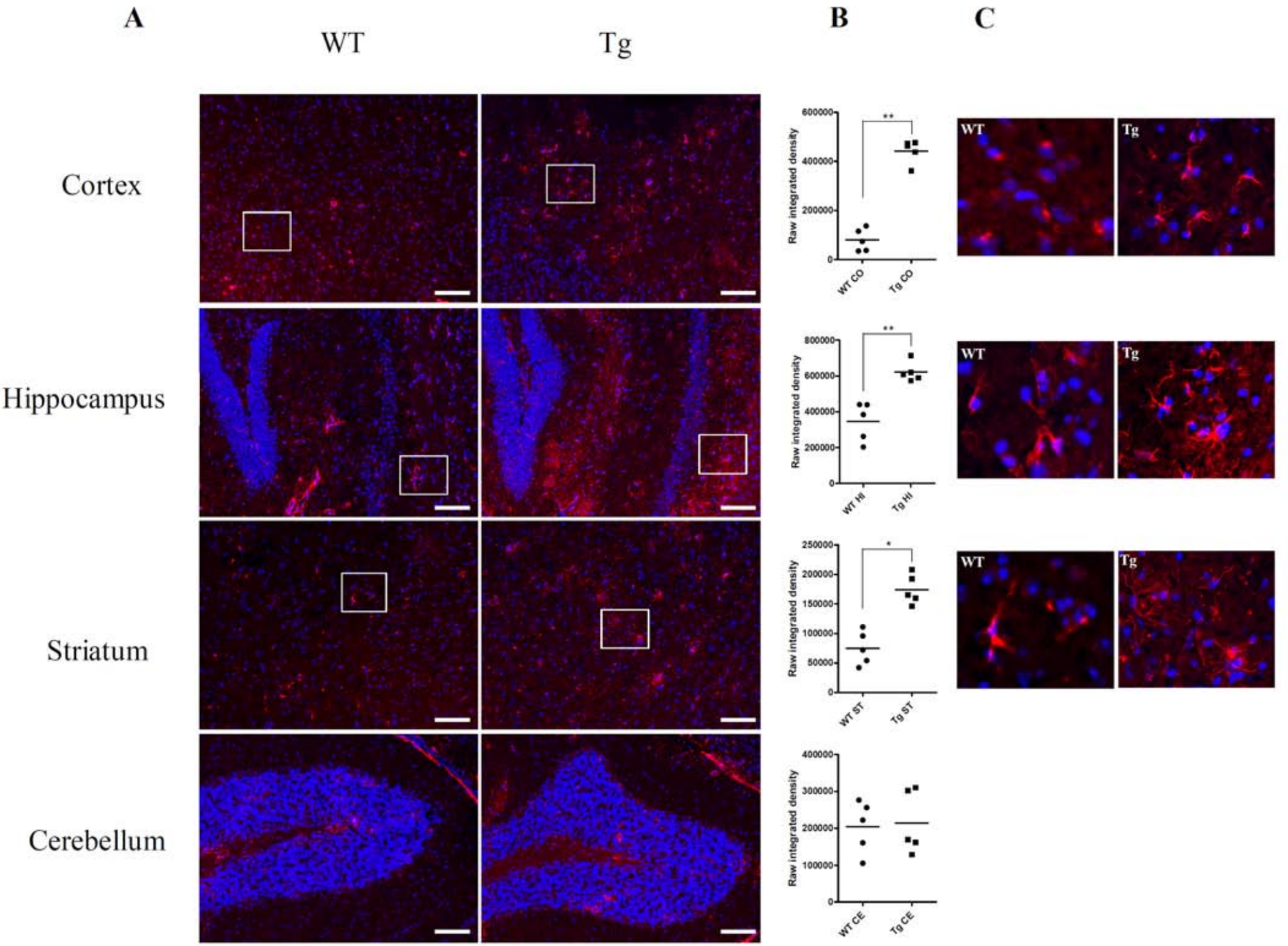
A
WT
Tg
B
C
Cortex
Hippocampus
Striatum
Cerebellum
Raw integrated density
600000
400000
200000
0
**
WT CO
Tg CO
800000
600000
400000
200000
0
**
WT HI
Tg HI
250000
200000
150000
100000
50000
0
*
WT ST
Tg ST
400000
300000
200000
100000
0
WT CE
Tg CE
WT
Tg
WT
Tg
WT
Tg

Figure 6

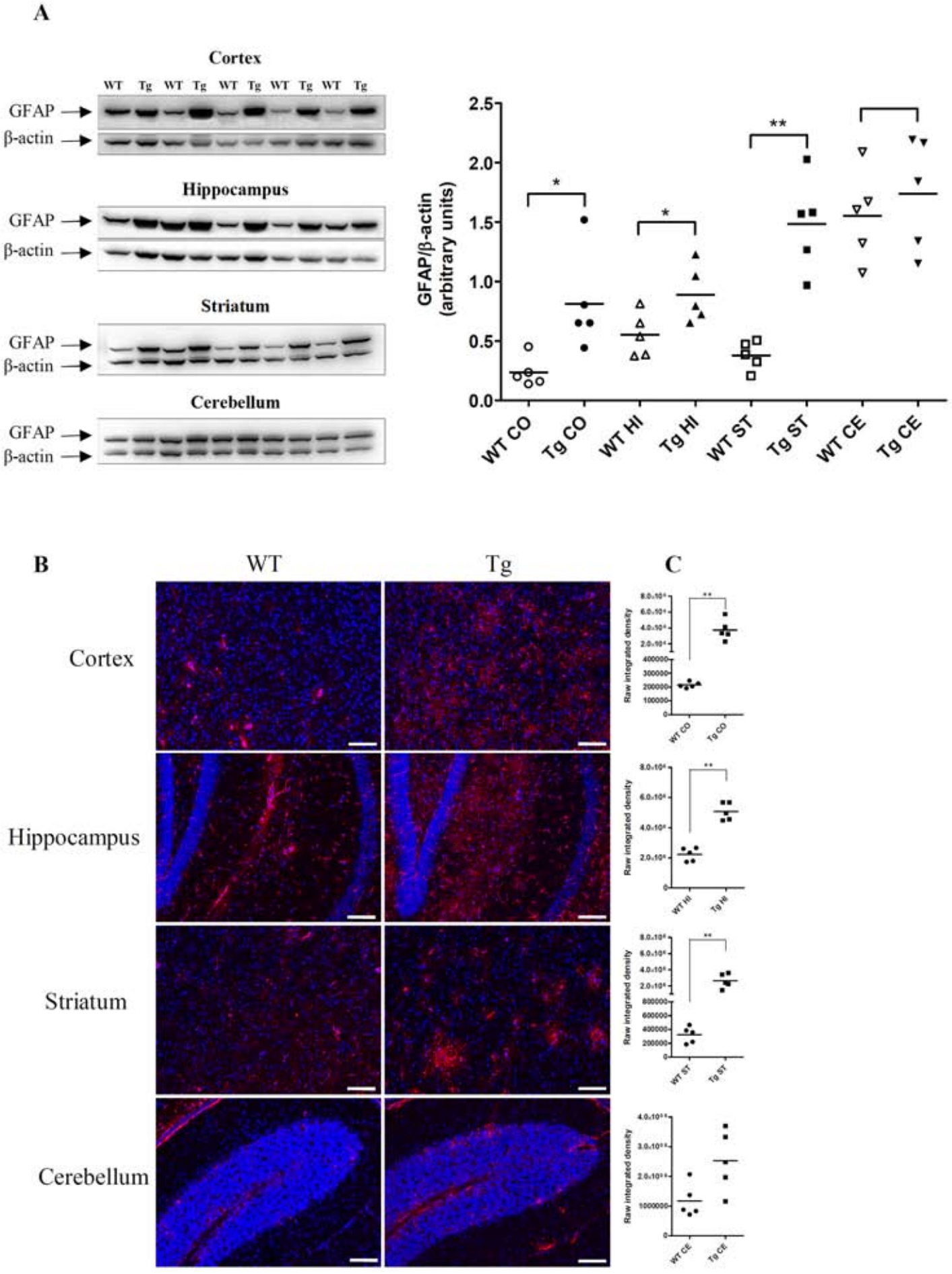
A
Cortex
WT Tg WT Tg WT Tg WT Tg WT Tg
GFAP
β-actin
Hippocampus
GFAP
β-actin
Striatum
GFAP
β-actin
Cerebellum
GFAP
β-actin
GFAP/β-actin (arbitrary units)
2.5
2.0
1.5
1.0
0.5
0.0
*
*
**
WT CO
Tg CO
WT HI
Tg HI
WT ST
Tg ST
WT CE
Tg CE
B
WT
Tg
Cortex
Hippocampus
Striatum
Cerebellum
C
Raw integrated density
WT CO
Tg CO
WT HI
Tg HI
WT ST
Tg ST
WT CE
Tg CE

Highlights

- This is the first longitudinal PET study for TSPO and amyloid in APPswePS1dE9 mice
- The cortex was affected earliest by β-amyloid plaques and rising in TSPO density
- At 19 months-of-age extensive in vitro studies of inflammation and A-β were performed
- The cortex, hippocampus and striatum were affected at this advanced stage of disease

Supplementary file 1

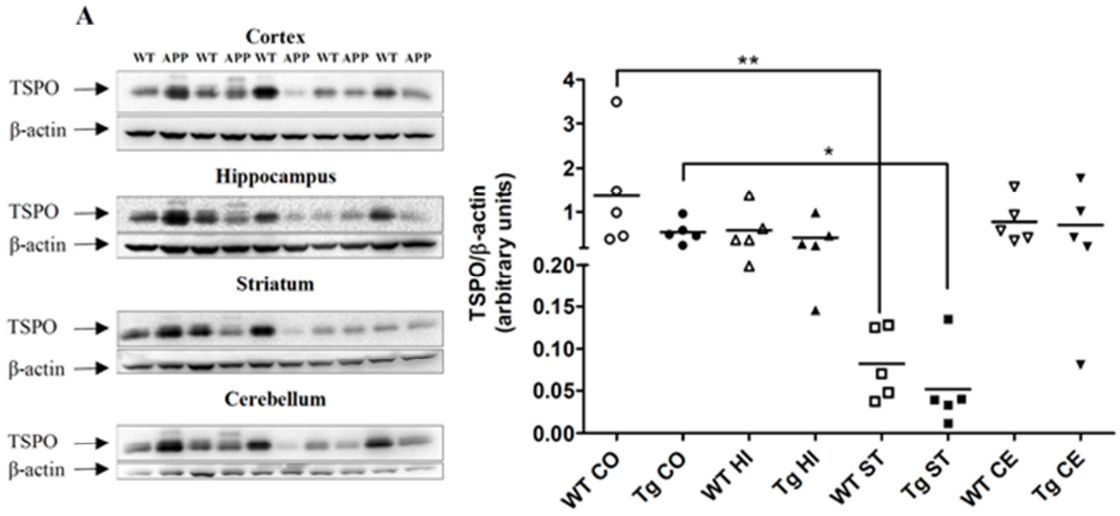

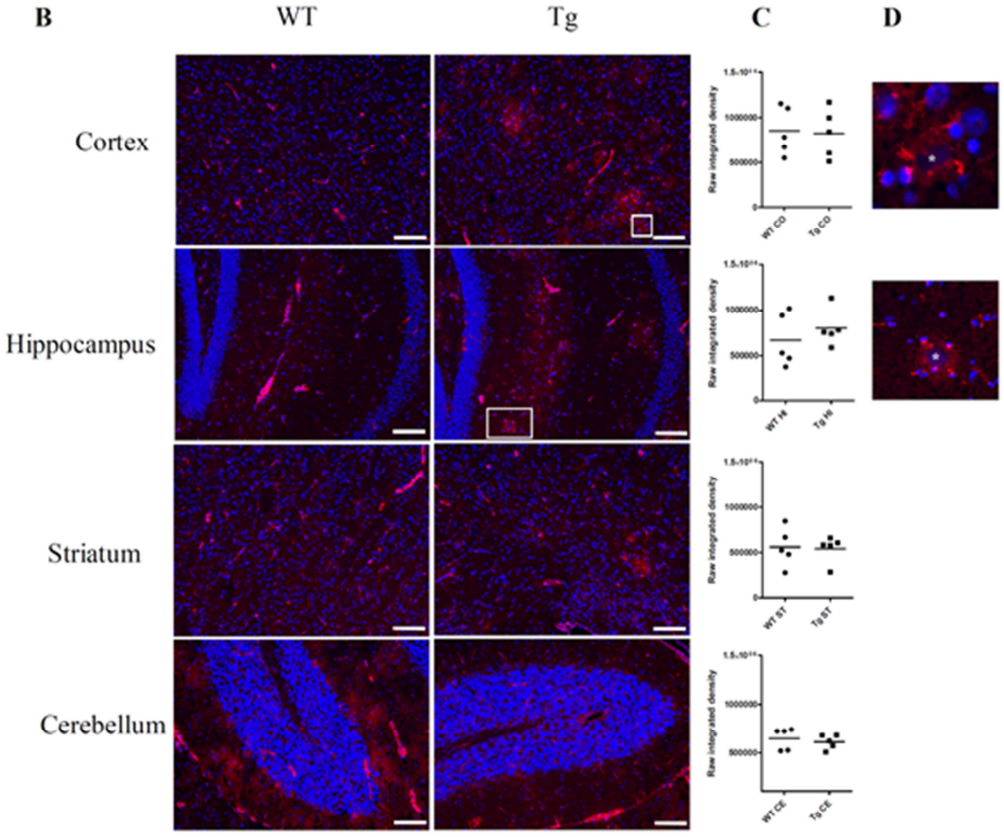

Immunoreactivity of TSPO in WT and Tg mice.

Panel A: representative immunoblots showed the immunoreactivity of TSPO in cortex (CO), hippocampus (HI), striatum (ST) and cerebellum (CE) of 19-months old WT and APPswePS1dE9 (Tg) mice. Semi-quantitative analysis of immunoblot was performed using Gene Tools software (Syngene, Ozyme France). The immunoreactivity of protein was normalized to β-actin immunoreactivity. The results are expressed as arbitrary units. Results are mean ± SEM for 5 mice in each group. $^{*}p < 0.05$, $^{**}p < 0.01$ compared to striatal TSPO in WT and Tg mice by Kruskal-Wallis test with a Dunns multiple comparison test. **Panel B:** representative confocal images of TSPO (red channel) and DAPI (blue channel) in cortex, hippocampus, striatum and cerebellum of 19-months old WT and Tg mice. Scale bar: 23 μm.

Panel C: Integrated density (product of Area and Mean Gray Value) was defined by using Image J software 1.47V. Scatter dot plot was shown and line represented mean. **Panel D:** magnified image of region of interest surrounded by white square in Tg image. Asterisks indicated amyloid deposits.

As shown in this figure, the immunoreactivity of TSPO (panel A) was similar in WT and Tg groups in each brain area except in the striatum where TSPO expression was significantly lower than that measured in the cortex both in WT and APPswePS1dE9 mice (16.82 and 10.78 times lower for WT and Tg mice, respectively). In addition, confocal staining also showed that the level of TSPO expression was identical in APPswePS1dE9 and wild-type mice (panels B and C). The TSPO signal is very marked in the blood vessels. In APPswePS1dE9 mice, a TSPO signal was also detected in cells located around amyloid plaques particularly in the cortex and hippocampus (magnified image in panel D).

Supplementary file 2: Correlation between amyloid and inflammatory data at 19 months by using Spearman test.

Table 1: Correlations between [^{18}F]AV-45 and [^{18}F]DPA-714 uptake values (SUVr)

Cortex		Hippocampus		Striatum	
rho	p	rho	p	rho	p
0.8424	**0.0037**	0.8788	**0.0016**	0.2121	0.5603

Table 2: Correlations between [^{18}F]AV-45 uptake values (SUVr) and raw integrated density of W02, GFAP, CD68 and of [^{3}H]PK-11195 binding values

	Cortex		Hippocampus		Striatum	
	rho	p	rho	p	rho	p
W02	0.7805	**0.0105**	0.9273	**0.0003**	-0.1515	0.6821
GFAP	0.7576	**0.0149**	0.8061	**0.0072**	-0.1879	0.6073
CD68	0.7939	**0.0088**	0.7091	**0.0268**	0.0060	1.0000
[^{3}H]PK-11195	0.9152	**0.0005**	0.8061	**0.0072**	0.1152	0.7589

Table 3: Correlations between [^{18}F]DPA-714 uptake values (SUVr) and raw integrated density of W02, GFAP, CD68 and of [^{3}H]PK-11195 binding values

	Cortex		Hippocampus		Striatum	
	rho	p	rho	p	rho	p
W02	0.6970	**0.0300**	0.9030	**0.0008**	0.4545	0.1912
GFAP	0.6242	0.0603	0.7697	**0.0126**	0.5879	0.0806
CD68	0.8182	**0.0058**	0.7818	**0.0105**	0.7333	**0.0202**
[^{3}H]PK-11195	0.7455	**0.0174**	0.8061	**0.0072**	0.5046	0.1440

Table 4: Correlations between [^{3}H] PK-11195 binding values and raw integrated density of W02, GFAP and CD68

	Cortex		Hippocampus		Striatum	
	rho	p	rho	p	rho	p
W02	0.7052	**0.0268**	0.8909	**0.0011**	0.6485	**0.0490**
GFAP	0.7903	**0.0088**	0.7333	**0.0202**	0.7939	**0.0088**
CD68	0.8024	**0.0072**	0.7333	**0.0202**	0.6848	**0.0347**

Table 5: Correlations between raw integrated densities of W02, GFAP and CD68

	Cortex		Hippocampus		Striatum	
	rho	p	rho	p	rho	p
GFAP	0.6606	**0.0438**	0.8545	**0.0029**	0.8667	**0.0022**
CD68	0.8061	**0.0072**	0.7697	**0.0126**	0.6970	**0.0306**